Low-Power Photothermal Probing of Single Plasmonic Nanostructures with Nanomechanical String Resonators

Schmid, Silvan; Wu, Kaiyu; Larsen, Peter Emil; Rindzevicius, Tomas; Boisen, Anja

Published in:
Nano Letters

Link to article, DOI:
10.1021/nl4046679

Publication date:
2014

Document Version
Publisher's PDF, also known as Version of record

NANO LETTERS

Letter

pubs.acs.org/NanoLett

Low-Power Photothermal Probing of Single Plasmonic Nanostructures with Nanomechanical String Resonators

Silvan Schmid,* Kaiyu Wu, Peter Emil Larsen, Tomas Rindzevicius, and Anja Boisen

Department of Micro- and Nanotechnology, Technical University of Denmark, DTU Nanotech, DK-2800, Kgs Lyngby, Denmark

Supporting Information

ABSTRACT: We demonstrate the direct photothermal probing and mapping of single plasmonic nanostructures via the temperature-induced detuning of nanomechanical string resonators. Single Au nanoslits and nanorods are illuminated with a partially polarized focused laser beam (λ = 633 nm) with irradiances in the range of 0.26−38 $\mu W/\mu m^2$. Photothermal heating maps with a resolution of ∼375 nm are obtained by scanning the laser over the nanostructures. Based on the string sensitivities, absorption efficiencies of 2.3 ± 0.3 and 1.1 ± 0.7 are extracted for a single nanoslit (53 nm × 1 μm) and nanorod (75 nm × 185 nm). Our results show that nanomechanical resonators are a unique and robust analysis tool for the low-power investigation of thermoplasmonic effects in plasmonic hot spots.

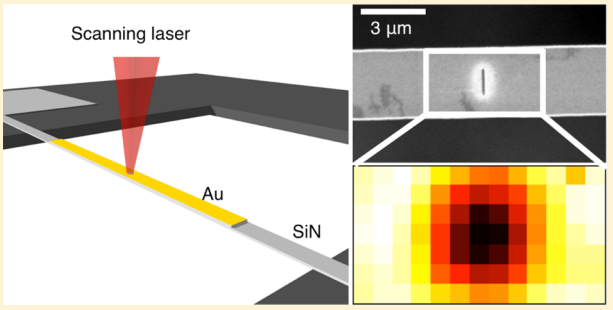

KEYWORDS: *Plasmonic hot spots, thermoplasmonics, nanomechanical resonators, optical heating, photothermal mapping*

Subwavelength noble metal structures (nanoparticles or nanovoids) support localized surface plasmon (LSP) resonances that usually occur in the visible and near-infrared spectral region. The incident light can couple to LSP modes producing extremely large field enhancements, so-called hot spots. These strong field confinements are prominently utilized e.g. in surface-enhanced Raman scattering (SERS) spectroscopy,[1−4] in plasmonic solar cells,[5−9] or as nano heat sources with a wide range of potential applications.[10−12] When a plasmonic nanostructure is illuminated with an incident light, part of it is scattered into the surrounding medium, while the other part is absorbed and dissipated as heat. Interestingly, optical and thermal hot spots are generally mismatched. Baffou et al. have shown experimentally that heat is concentrated in areas where charges can freely flow, while optical hot spots usually appear at the metal interface with the greatest charge accumulation (tip effect).[10] So far there have been a few attempts to investigate the photothermal heating of metal nanostructures using thermal-optical[13] and thermoresistive[14] techniques and an AFM tip.[15] However, the desirable direct investigation of the heating mechanisms in plasmonic structures is still a challenge due to the lack of robust experimental tools.[10] Herein we propose a new approach to probe and image plasmonic structures with submicrometer resolution by measuring the photothermally induced frequency detuning of highly temperature sensitive nanomechanical resonators. It has been shown that plasmons can be coupled to the vibration of a nanomechanical resonator.[16] We employ the high temperature sensitivity of a nanomechanical string resonator[17,18] to directly probe the heating pattern produced by single Au nanoslits and nanorods illuminated by a partially polarized scanning laser beam. The experimental approach allows a sensitive heat mapping of nobel metal nanostructures to study heat generation and thermal diffusion in e.g. plasmonic hot spots.

The proposed method to photothermally probe plasmonic nanostructures is schematically illustrated in Figure 1. Single Au nanoslits and nanorods were chosen as a nano heat source. The

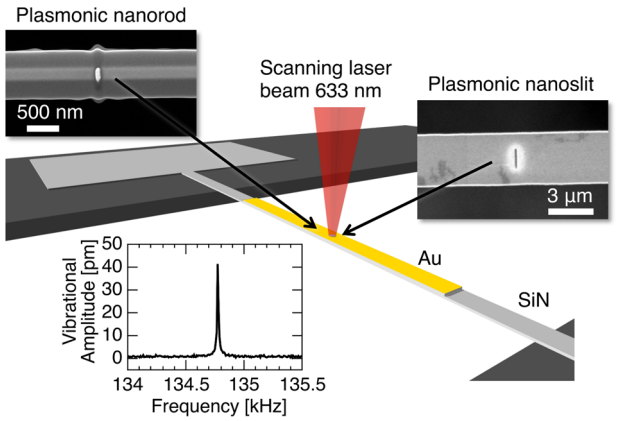

Figure 1. Schematic depiction of the experimental setup. A nanomechanical SiN string resonator is partially coated with a Au layer. A plasmonic nanoslit or nanorod (etched with a focused ion beam) is located in the string center and probed with a low-power focused laser beam from a laser-Doppler vibrometer. The inset shows the thermal fluctuation spectrum of a 900 μm long micromechanical SiN string resonator.

Received: December 17, 2013
Revised: March 19, 2014

   dx.doi.org/10.1021/nl4046679 | *Nano Lett.* XXXX, XXX, XXX−XXX

nanostructures were milled using a focused ion beam (FIB) (using a 30 keV Ga^+ beam with current of 9 pA) into the Au metal coating of a nanomechanical silicon nitride (SiN) string resonator. The fabrication of the SiN string resonators is described elsewhere.[19] The string resonance frequency corresponds to the thermal vibration of the string (see inset of Figure 1), measured in high vacuum with a laser-Doppler vibrometer (MSA-5 from Polytec). The partially polarized vibrometer's laser beam (λ = 633 nm, full width at half-maximum fwhm = 0.9 μm with 50× objective) is utilized to simultaneously record the string resonance frequency and excite localized and surface plasmons in individual Au nanoslits and nanorods. Minimal and maximal irradiances of I = 0.26−8.3 $\mu W/\mu m^2$ and I = 1.1−38 $\mu W/\mu m^2$ with the 20× and 50× objective, respectively, were used. Part of the incident light is absorbed by a nanostructure and dissipated into heat. The string resonator is highly temperature sensitive and can be used to monitor the photothermal heating produced by the nano heat source on the string via the resonance frequency detuning.

In vacuum and for low photothermal heating, the absorbed energy from a nanostructure is transferred off a string mainly by thermal conduction. In this case, the relative frequency change δf per absorbed power P in the center of a string resonator is given by[20]

$$\delta f/P = -\frac{L}{16wh}\frac{\alpha E}{\sigma\kappa} \quad (1)$$

with the string length L, thickness h, width w, thermal expansion coefficient α, Young's modulus E, tensile prestress σ, and thermal conductivity κ. From eq it can be seen that the sensitivity is highest for long and slender strings with a low thermal conductivity. In order to improve the sensitivity, the highly conductive Au film was removed by FIB milling at the anchors of some strings.

The absolute value of the electric field around a 2-dimensional (infinitely long) Au nanoslit was simulated using the finite element method (FEM). Figure 2a shows the $|E|$ map in a string cross section for s-polarized (perpendicular) and p-polarized (parallel) incident light with respect to the nanoslit orientation. In the s-polarized case the incoming field is enhanced around the slit due to the localized nature of the plasmonic excitation. Additionally, a surface plasmon polariton (SPP) is launched at the metal−insulator interface. In the p-polarized mode, the LSP generation is minimized. The resistive loss and thus the heating in the metal of a string is roughly 5 times larger for s-polarization compared to p-polarization. The polarization-dependent photoinduced heating of the string resonator is tested using three identical nanoslits with different orientations as shown in Figure 2b. Photothermal maps around vertically and horizontally aligned single nanoslits are shown in Figure 2c, and the spatial resolution is ~375 nm. According to eq 1, the thermal heating is directly proportional to the measured relative frequency shift δf of the string resonator. In the s-polarization case, the produced frequency shift, and thus the heat, is roughly double in magnitude compared to the p-polarization case. The laser beam is partially polarized with a power ratio of 4:1 in the two directions of polarization. With the heating ratio 5:1 of s- vs p-polarization, all heating contributions from both polarization directions add up to a total heating ratio of 21:9 (see Figure 2d). This is well in agreement with the measured double frequency detuning of s-polarization compared to p-polarization. A line scan over all three slits is depicted in Figure 2e, showing the continuous

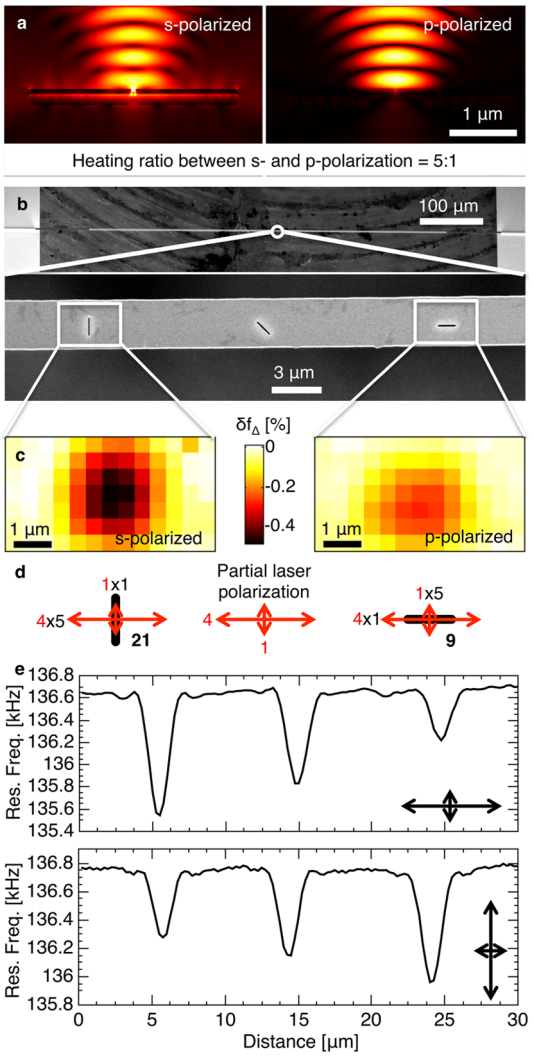

Figure 2. (a) FEM simulation of the modulus amplitude of the electric field (ranged from 0 to 2 V/m) for a SiN string (157 nm thick and 3 μm wide) covered with 80 nm Au. (b) SEM image of a Au-coated stoichiometric SiN string (σ = 900 MPa, L = 900 μm, w = 3 μm, h = 157 nm, covered with 80 nm Au), featuring plasmonic nanoslits in the center (90 nm wide and 1 μm long). (c) Photothermal maps of a vertical and horizontal plasmonic slit with a partially horizontally polarized laser beam (using 50× objective) with an irradiance of I = 11 $\mu W/\mu m^2$. (d) Schematic calculation of the heating ratio between a vertical and horizontal nanoslit. (e) Resonance frequency of the string for a scan over all three plasmonic nanoslits for two perpendicular laser orientations with I = 25 $\mu W/\mu m^2$.

polarization-dependent heating for three different nanoslit orientations. The observed polarization dependence is clear evidence of the plasmonic nature of the absorption enhancement of the Au nanoslits.

Figure 3 shows the photothermal heating as a function of laser power of a single plasmonic nanoslit (see Figure 3a) on a 1 μm wide nanomechanical string. Figure 3b shows the relative resonance frequency δf of the string when focusing the laser beam either directly on the Au nanoslit or planar gold film. In order to achieve an even illumination of the 1 μm long slit, the measurements were done with the 20× objective. The relative frequency difference δf_Δ, as shown in Figure 3c, is directly caused by the additional photothermal heating of the plasmonic nanoslit. From the slope, a sensitivity of $\delta f_\Delta/I = -0.3 \pm 0.03\%/$

dx.doi.org/10.1021/nl4046679 | Nano Lett. XXXX, XXX, XXX−XXX

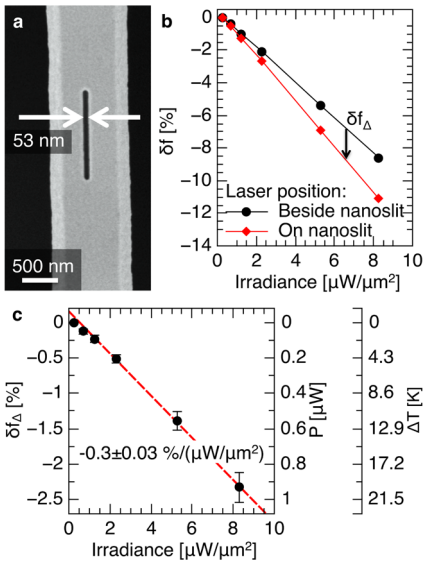

Figure 3. (a) SEM image of nanoslit in the center of a silicon-rich SiN nanostring (σ = 200 MPa, L = 550 μm, w = 1 μm, h = 220 nm, covered with 50 nm Au). (b) Measured relative resonance frequency of this nanostring as a function of laser irradiance when focused on the plasmonic nanoslit and when focused beside the nanoslit (using 20× objective). (c) Difference of the relative resonance frequency δf_Δ caused by the photothermal heating of the plasmonic nanoslit. The right y-axis further shows the power P absorbed by the nanoslit and the resulting local temperature increase ΔT. The error bars represent the standard deviation of three measurements.

(μW/μm^2) can be extracted. With a sensitivity of the nanostring of $\delta f/P$ = −2.51 ± 0.13%/μW (see Supporting Information), this results in an absorption cross section of P/I = 0.12 ± 0.01 μm^2. This corresponds to an absorption efficiency of 2.3 ± 0.3 for the nanoslit with a geometrical area of 0.053 μm^2. The local temperature in the center of the nanostring increases by $\Delta T/P$ = 21.5 ± 3.2 K/μW (see Supporting Information), which results in a nanoslit-induced heating per irradiated light of $\Delta T/I$ = 2.6 ± 0.5 K/(μW/μm^2). Both the absorbed power P and the local temperature increase ΔT are plotted on the right y-axis of Figure 3c.

As a comparison to the plasmonic nanoslits which excite both LSPs and SPPs (see Figure 2a) we probed a plasmonic Au nanorod which only supports LSPs. Figure 4a shows the SEM image of a nanorod etched in the Au coating of a 1 μm wide nanomechanical string. The photothermal maps around the Au nanorod for s-polarization (top) and p-polarization (bottom) are shown in Figure 4b. In the s-polarized map, the distinct heating pattern of the nanorod is clearly visible whereas in the p-polarized map it is indiscriminable from the background. The nanorod has an LSP resonance close to 633 nm along its short side, as can be seen from Figure 4c, whereas the absorption efficiency has a minimum along its long side. This measurements indicates the photothermal detection of a single nanorod via its LSP. From the relative frequency change δf_Δ caused by the Au nanorod, shown in Figure 4d (similar to Figure 3c), a sensitivity of $\delta f_\Delta/I$ = −90 ± 60 ppm/(μW/μm^2) can be extracted. From the string sensitivities of $\delta f/P$ = −6.1 ± 0.5 ppm/nW and $\Delta T/P$ = 12.7 ± 1.9 K/μW (see Supporting Information), it is possible to calculate the absorption cross-section P/I = 0.015 ± 0.010 μm^2 and temperature increase per irradiance $\Delta T/I$ = 0.19 ± 0.13 K/(μW/μm^2). Both the absorbed power P and the local temperature increase ΔT are

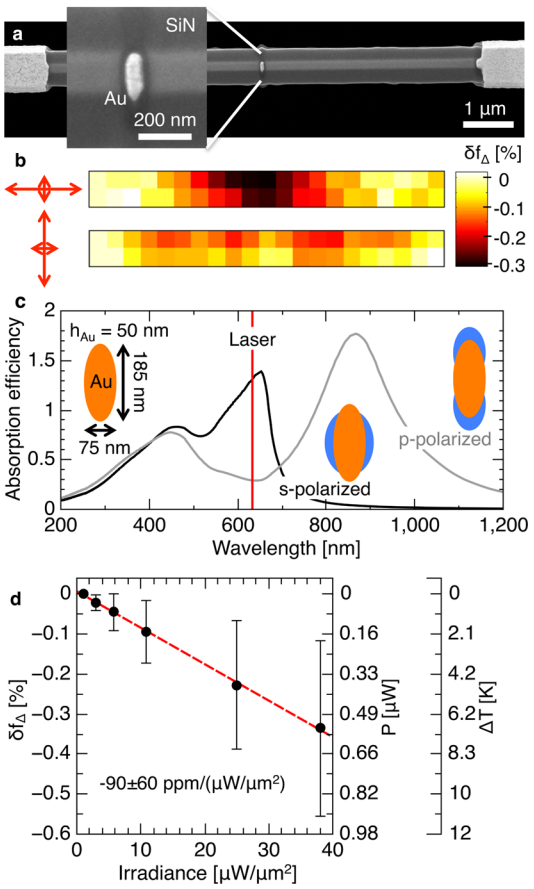

Figure 4. (a) SEM image of a plasmonic Au nanorod (50 nm thick, 75 nm wide, and 185 nm long) located at the center of a silicon-rich SiN nanostring (σ = 200 MPa, L = 550 μm, w = 1 μm, h = 220 nm, covered with 50 nm Au). (b) Photothermal maps of a vertical plasmonic nanorod with a partially horizontally and vertically polarized laser beam with an irradiance of I = 38 μW/μm^2 (using 50× objective). (c) Effective absorption of a single Au nanorod modeled as a point-like electric dipole (see Supporting Information). (d) Difference of the relative resonance frequency δf_Δ caused by the photothermal heating of the plasmonic nanorod. The right y-axis further shows the power P absorbed by the nanorod and the resulting local increase in temperature ΔT. The error bars represent the standard deviation of six measurements.

plotted on the right y-axis of Figure 4d. From the absorption cross section an absorption efficiency of 1.1 ± 0.7 can be calculated for the nanorod with a geometrical area of 0.014 μm^2. This corresponds well with the calculated absorption efficiency of 1.3 as depicted in Figure 4c, and it is roughly half the absorption efficiency of the nanoslit. This difference can mainly be assigned to the additional SPPs launched at the nanoslit which contributes strongly to the overall absorption.

The typical irradiances used in this experiment of a few μW/μm^2 is 1−4 orders of magnitude lower than the illuminances typically used in state-of-the-art probing of plasmonic nanostructures.[11,13,14] Low irradiances are critical for studying thermal hot spots with (bio)molecules adsorbed on the metal surface to avoid photochemistry related effects or thermal decomposition of adsorbates.

In conclusion, we demonstrate the low-power photothermal probing and mapping of single plasmonic Au nanoslits and nanorods via the temperature-induced detuning of the resonance frequency of nanomechanical SiN string resonators.

dx.doi.org/10.1021/nl4046679 | Nano Lett. XXXX, XXX, XXX−XXX

The polarization-dependent heating patterns are mainly observed in the vicinity of the nanostructures that can be attributed to excited LSPs and the additional SPPs at the Au/SiN interface of the nanoslits. We produced a photothermal map with a resolution of ~375 nm by scanning the focused probing laser over the nanostructure area. Based on the string sensitivies, absorption efficiencies of 2.3 ± 0.3 and 1.1 ± 0.7 for a nanoslit (53 nm × 1 μm) and nanorod (75 nm × 185 nm), respectively, were extracted. The increased absorption of the nanoslit can be assigned to the additional excitation of LSPs. Our results show that nanomechanical resonators are a unique and robust tool for probing thermal effects in plasmonic nanostructures.

■ ASSOCIATED CONTENT

Supporting Information

String sensitivity calculations and nanorod dipole model. This material is available free of charge via the Internet at http://pubs.acs.org.

■ AUTHOR INFORMATION

Corresponding Author

*E-mail: sils@nanotech.dtu.dk (S.S.).

Notes

The authors declare no competing financial interest.

■ ACKNOWLEDGMENTS

This research is supported by the Villum Foundation's Young Investigator Program (Project No. VKR023125) and The Danish Council for Independent Research (NAPLAS -Nanoplasmonic Sensors). The authors thank Zoltán Imre Balogh and Adam Fuller for the support with the focused ion beam milling and Jens Q. Adolphsen for the cleanroom support.

■ REFERENCES

(1) Nie, S.; Emory, S. R. *Science* **1997**, *275*, 1102−1106.
(2) Kneipp, K.; Wang, Y.; Kneipp, H.; Perelman, L.; Itzkan, I.; Dasari, R.; Feld, M. *Phys. Rev. Lett.* **1997**, *78*, 1667−1670.
(3) Haynes, C. L.; Mcfarland, A. D.; Duyne, R. P. V. *Anal. Chem.* **2005**, *77*, 338A−346A.
(4) Moskovits, M. *J. Raman Spectrosc.* **2005**, *36*, 485−496.
(5) Atwater, H. A.; Polman, A. *Nat. Mater.* **2010**, *9*, 205−213.
(6) Pillai, S.; Catchpole, K. R.; Trupke, T.; Green, M. A. *J. Appl. Phys.* **2007**, *101*, 093105.
(7) Catchpole, K. R.; Polman, A. *Opt. Express* **2008**, *16*, 21793−21800.
(8) Ferry, V. E.; Verschuuren, M. A.; Li, H. B. T.; Verhagen, E.; Walters, R. J.; Schropp, R. E. I.; Atwater, H. A.; Polman, A. *Opt. Express* **2010**, *18*, A237−A245.
(9) Derkacs, D.; Lim, S. H.; Matheu, P.; Mar, W.; Yu, E. T. *Appl. Phys. Lett.* **2006**, *89*, 093103.
(10) Baffou, G.; Quidant, R. *Laser Photonics Rev.* **2013**, *7*, 171−187.
(11) Baffou, G.; Quidant, R.; Garca de Abajo, F. J. *ACS Nano* **2010**, *4*, 709−716.
(12) Schuller, J. A.; Barnard, E. S.; Cai, W.; Jun, Y. C.; White, J. S.; Brongersma, M. L. *Nat. Mater.* **2010**, *9*, 193−204.
(13) Baffou, G.; Girard, C.; Quidant, R. *Phys. Rev. Lett.* **2010**, *104*, 136805.
(14) Herzog, J. B.; Knight, M. W.; Natelson, D. *Nano Lett.* **2014**, *14*, 499−503.
(15) Lahiri, B.; Holland, G.; Aksyuk, V.; Centrone, A. *Nano Lett.* **2013**, *13*, 3218−3224.
(16) Thijssen, R.; Verhagen, E.; Kippenberg, T. J.; Polman, A. *Nano Lett.* **2013**, *13*, 3293−3297.
(17) Larsen, T.; Schmid, S.; Villanueva, L. G.; Boisen, A. *ACS Nano* **2013**, *7*, 6188−6193.
(18) Larsen, T.; Schmid, S.; Gronberg, L.; Niskanen, A. O.; Hassel, J.; Dohn, S.; Boisen, A. *Appl. Phys. Lett.* **2011**, *98*, 121901.
(19) Schmid, S.; Jensen, K. D.; Nielsen, K. H.; Boisen, A. *Phys. Rev. B* **2011**, *84*, 165307.
(20) Yamada, S.; Schmid, S.; Larsen, T.; Hansen, O.; Boisen, A. *Anal. Chem.* **2013**, *85*, 10531−10535.